Monthly Notices
of the
ROYAL ASTRONOMICAL SOCIETY

Mon. Not. R. Astron. Soc. **415,** 271–278 (2011) doi:10.1111/j.1365-2966.2011.18694.x

Flow-driven cloud formation and fragmentation: results from Eulerian and Lagrangian simulations

Fabian Heitsch,[1,2,3⋆] Thorsten Naab[3,4⋆] and Stefanie Walch[3,5⋆]

[1]*Department of Physics and Astronomy, UNC Chapel Hill, 120 E Cameron St, Chapel Hill, NC 27599-3255, USA*
[2]*Department of Astronomy, University of Michigan, 500 Church St, Ann Arbor, MI 48109-1042, USA*
[3]*Universitäts Sternwarte München, Scheinerstr. 1, D-81679 München, Germany*
[4]*Max Planck Institut für Astrophysik, Karl-Schwarzschild-Str. 1, 85741 Garching, Germany*
[5]*School of Physics and Astronomy, Cardiff University, 5 The Parade, Cardiff CF24 3AA*

Accepted 2011 March 11. Received 2011 February 24; in original form 2010 October 31

ABSTRACT

The fragmentation of shocked flows in a thermally bistable medium provides a natural mechanism to form turbulent cold clouds as precursors to molecular clouds. Yet because of the large density and temperature differences and the range of dynamical scales involved, following this process with numerical simulations is challenging. We compare two-dimensional simulations of flow-driven cloud formation without self-gravity, using the Lagrangian smoothed particle hydrodynamics (SPH) code VINE and the Eulerian grid code PROTEUS. Results are qualitatively similar for both methods, yet the variable spatial resolution of the SPH method leads to smaller fragments and thinner filaments, rendering the overall morphologies different. Thermal and hydrodynamical instabilities lead to rapid cooling and fragmentation into cold clumps with temperatures below 300 K. For clumps more massive than 1 $M_\odot$ pc^{-1}, the clump mass function has an average slope of −0.8. The internal velocity dispersion of the clumps is nearly an order of magnitude smaller than their relative motion, rendering it subsonic with respect to the internal sound speed of the clumps but supersonic as seen by an external observer. For the SPH simulations most of the cold gas resides at temperatures below 100 K, while the grid-based models show an additional, substantial component between 100 and 300 K. Independent of the numerical method, our models confirm that converging flows of warm neutral gas fragment rapidly and form high-density, low-temperature clumps as possible seeds for star formation.

Key words: hydrodynamics – instabilities – methods: numerical – stars: formation – ISM: clouds – ISM: kinematics and dynamics.

1 INTRODUCTION

The highly filamentary morphology of molecular clouds (MCs) and their observed non-thermal linewidths (Falgarone & Phillips 1990; Williams, Blitz & McKee 2000) point to MCs being highly dynamical objects. Observational evidence suggests that star formation in local MCs such as Taurus is rapid once molecular gas is available and that the parental clouds are short-lived (Elmegreen 2000; Hartmann, Ballesteros-Paredes & Bergin 2001; Hartmann 2003). The dynamical, or turbulent, nature of MCs is assumed to play a crucial role in the process of star formation via turbulent fragmentation (Larson 1981; Mac Low & Klessen 2004, see also Ballesteros-Paredes 2006, for a summary of the effects and interpretation of turbulence in MCs).

⋆E-mail: fheitsch@unc.edu (FH); naab@mpa-garching.mpg.de (TN); stefanie.walch@astro.cf.ac.uk (SW)

Because of the rapid onset of star formation, the cloud formation process needs to provide the MC with the observed turbulence and substructure. Moreover, global geometry and gravity considerations mandate that this substructure be non-linear (Burkert & Hartmann 2004), i.e. a physical process is needed that can imprint non-linear density perturbations in the protocloud during its formation. These requirements have led to the scenario of flow-driven cloud formation, where MCs are assembled by large-scale converging flows of atomic hydrogen corresponding to the warm neutral medium (Ballesteros-Paredes, Hartmann & Vázquez-Semadeni 1999; Hartmann et al. 2001; Hartmann 2003; see also Elmegreen 1993, 2000). The rapid fragmentation is driven by a combination of strong thermal and dynamical instabilities, dominated by the thermal instability [TI; Field 1965; see also Heitsch, Hartmann & Burkert 2008b for a discussion of time-scales].

Large-scale gas flows are ubiquitous in the Galaxy. They might be driven locally by supernova explosions (Elmegreen & Lada 1977; McCray & Kafatos 1987; Nigra et al. 2008) or globally by shear

© 2011 The Authors
Monthly Notices of the Royal Astronomical Society © 2011 RAS

motions in the Galactic disc, global gravitational instabilities (Yang et al. 2007), gas infall from the halo (Mirabel 1982; Lacey & Fall 1985), interactions with the central bar (Roberts, Huntley & van Albada 1979; Combes & Gerin 1985) or satellite galaxies. On extragalactic scales collisions of galactic discs trigger gas flows, shocks and starbursts (Mihos & Hernquist 1996; Naab, Jesseit & Burkert 2006; Karl et al. 2010).

High-resolution simulations in two (Audit & Hennebelle 2005; Heitsch et al. 2005, 2006; Hennebelle & Audit 2007; Hennebelle, Audit & Miville-Deschênes 2007) and three dimensions (Vázquez-Semadeni et al. 2006, 2007; Heitsch et al. 2008a; Hennebelle et al. 2008; Banerjee et al. 2009) have demonstrated that the flow-driven formation of clouds is indeed a natural and elegant way to provide the clouds with the observed turbulence and substructure. Except for Vázquez-Semadeni et al. (2007), the above authors used various grid-based methods. However, due to the high-density contrast and the strong TI in the intermediate-temperature regime between 300 $< T <$ 5000 K, the spatial scales of the forming cold filaments and clumps shrink dramatically. This problem becomes even more severe with gravity acting upon the cold regions.

Due to its Lagrangian nature, the strength of smoothed particle hydrodynamics (SPH; e.g. Monaghan 1992) resides in its capability to follow fluid flows at 'arbitrary' spatial resolution. In particular, dissipative properties of SPH methods do not depend on the geometry or direction, which can cause issues for grid-based methods without physical dissipation control (Rampp, Mueller & Ruffert 1998). SPH has been used to model the interstellar medium on all scales, from planet formation (e.g. Mayer et al. 2002), formation of protostellar discs from rotating and turbulent cores (Walch et al. 2009, 2010), formation of stars and cores (Klessen 1997; Bate, Bonnell & Bromm 2003), ionization feedback from massive stars (Bisbas et al. 2009; Gritschneder et al. 2009, 2010), formation of MCs in galactic discs (Dobbs, Bonnell & Pringle 2006; Dobbs & Bonnell 2007; Dobbs et al. 2008) and galaxy evolution (Hernquist & Katz 1989; Steinmetz 1996; Springel 2000; Naab et al. 2006, 2007) to large-scale simulation of galaxy formation (e.g. Springel & Hernquist 2003). Vázquez-Semadeni et al. (2007) presented models of flow-driven MC formation using SPH. However, SPH has its own inherent limitations, among others a limited mass resolution and spatially varying dissipative properties. Hence, the question remains whether SPH and grid-based methods give similar results for a specific astrophysical problem and what the method-intrinsic differences are. Nagamine et al. (2005) showed for cosmological applications that both approaches give statistically similar results, and Klessen, Heitsch & Mac Low (2000) concluded the same for models of self-gravitating-driven turbulence in a periodic box of isothermal gas, although Kitsionas et al. (2009) showed for the latter application that SPH is more dissipative than grid models for decaying turbulence.

Yet it remains unclear whether this agreement between methods holds for models of a thermally unstable, turbulent interstellar medium. This is of particular interest as Agertz et al. (2007) and Junk et al. (2010) have pointed out SPH's limitations evolving shear flow instabilities (see, however, Price 2008; Read, Hayfield & Agertz 2010; Abel 2010) – a crucial ingredient in the formation of turbulent clouds from colliding flows (Heitsch et al. 2006, 2008b).

This paper compares the Eulerian and Lagrangian approach to the problem of flow-driven cloud formation in two dimensions. The concept of the simulations follows Heitsch et al. (2005, 2006) and is summarized in Section 2. We find (Section 3) a good agreement between SPH and grid-based results in terms of the rapid onset of fragmentation and, to a lesser degree, of morphology.

The total amount of mass accumulated in the cold gas component ($T < 300$ K) is smaller in the SPH models, yet the temperature distribution within the cold gas is concentrated towards lower temperatures. The grid models show a wider spread of temperatures but an overall higher mass in cold gas. We attribute this difference to the overcooling problem in SPH described by e.g. Pearce et al. (1999). Line-of-sight velocity dispersions as seen by an observer are generally supersonic with respect to the cold gas, yet the dispersions within the cores are approximately sonic, in agreement with observations (e.g. André et al. 2007). The strength of the Lagrangian approach is demonstrated when deriving the mass distribution of cold dense fragments forming in the colliding flows.

2 MODELS

All SPH simulations are run with the parallel shared memory SPH code VINE (Nelson, Wetzstein & Naab 2009; Wetzstein et al. 2009). The code solves the asymmetric form of the energy equation and uses the standard implementation of the artificial viscosity to treat shocks (Monaghan 1992). SPH particles have individual time-steps that can cover approximately eight orders of magnitude. The time-steps are determined by the local Courant–Friedrichs–Lewy criterion (Monaghan 1989) ensuring that information is not carried over length-scales larger than the local kernel size that is defined by the 20 nearest neighbour particles in two dimensions. In addition, we require that the fractional change of the kernel size of each particle is limited to 10 per cent. Thereby, we ensure that particles require several time-steps to pass through the interface of a strong shock.

For the fixed-grid simulations, we used the gas-kinetic grid code PROTEUS (Prendergast & Xu 1993; Slyz & Prendergast 1999; Xu 2001; Heitsch et al. 2004) in an identical implementation as described by Heitsch et al. (2008a). PROTEUS allows the explicit control of viscosity and heat conductivity at fixed spatial scales [see Slyz et al. (2002) for a detailed description].

2.1 Heating and cooling

To compute the heating and cooling rates, we have used the rates for optically thin atomic lines from Wolfire et al. (1995, 2003). The cooling curve covers a range of $10^{-2} \leq n \leq 10^3$ cm^{-3} in density and $30 \leq T \leq 2.5 \times 10^4$ K in temperature and is identical to that used by Heitsch et al. (2006). Dust extinction becomes important above column densities of $N(\mathrm{H\,I}) \approx 1.2 \times 10^{21}$ cm^{-2}, which are reached only in the densest regions modelled. Thus, we use the unattenuated ultraviolet radiation field for grain heating, expecting substantial uncertainties in cooling rates only for the densest regions. The ionization degree is derived from a balance between ionization by cosmic rays and recombination, assuming that Lyα photons are directly reabsorbed. As in Heitsch et al. (2006), heating and cooling are implemented iteratively as a source term for the internal energy e of the form

$$\frac{\mathrm{d}e}{\mathrm{d}t} = n\Gamma(T) - n^2\Lambda(T) \qquad (1)$$

in units of energy per volume per time. Here, Γ is the heating contribution (mainly photoelectric heating from grains) and $n\Lambda$ is the cooling contribution (mainly due to the C II line at 158 μm). To speed up the calculations, equation (1) is tabulated on a 2048^2 grid in density and temperature. For each cell and iteration, the actual energy change is then bilinearly interpolated from this grid.

The implementation of heating and cooling in VINE follows closely that for PROTEUS described above. For each particle i the change of

the specific internal energy, u, in units of energy per unit mass per unit time is computed as

$$n_i \frac{\mathrm{d}u_i}{\mathrm{d}t} = n_i \Gamma(T_i) - n_i^2 \Lambda(T_i). \quad (2)$$

If the current integration time-step of the particle is larger than 1 per cent of the local cooling time, the cooling is computed iteratively in steps of 1 per cent of the local cooling time. Using periodic boxes of constant density and temperature at different values, we have tested that this implementation results in the correct cooling rates.

2.2 Initial and boundary conditions

Two opposing, uniform, identical flows in the x–y computational plane initially collide head-on at a sinusoidal interface with wave number $k_y = 1$ and amplitude Δ (see fig. 1 in Heitsch et al. 2006). The incoming flows are in thermal equilibrium at a density of $n_0 = 1.0\,\mathrm{cm}^{-3}$, a temperature of $T_0 = 8.5 \times 10^3$ K and a velocity of 21 km s^{-1}, typical for parameters of the warm neutral medium. The box length is 44 pc.

We ran identical model sets with VINE (model names headed by 'V') and PROTEUS (names headed by 'P'). The model name V0256 specifies an SPH model with initially 256^2 particles, while e.g. P2048 denotes a grid model with 2048^2 cells.

Initially, we distribute the SPH particles on a grid in the square domain. The particle mass resolution is $7.2 \times 10^{-4}\,\mathrm{M}_\odot\,\mathrm{pc}^{-1}$. We create new particle layers at the x boundaries at the initial grid resolution with the appropriate velocities. Thus, the total particle number of the simulation is continuously increasing, starting with $256^2 = 65\,536$ particles. At 9 Myr, there are already 640 000 particles in model V0256. This leads to a significant slowing down as the simulation proceeds.

We use periodic boundary conditions in the y-direction. Heitsch et al. (2006) explored the effect of the choice of boundary conditions on the mass budget and the morphology of the forming clouds. They found that although open boundaries allow a small fraction of the gas to leave the simulation domain (or the active region), the total mass budget and the morphology are only slightly affected. The cooling time-scale is much shorter than the flow time-scale and the sound crossing time, so that the gas is compressed and cooled down before it can feel the boundaries. Only gas close to the boundaries will be affected.

3 RESULTS

3.1 Morphologies

We begin with the flow morphologies (Fig. 1), comparing density and temperature maps of models V0256 (left) and P1024 (right). Densities and temperatures have been scaled to the same ranges, and for both codes, the central quarter (22^2 pc^2) of the simulation domain is shown at times $t = 2.3$, 4.2 and 9.2 Myr after the initial flow contact. The most noticeable difference is the much more filigree structure of the cold gas exhibited in the SPH simulations. Comparing the initial resolution (256^2 versus 1024^2) against the effective resolution indicates the resolving power of the Lagrangian method. The smallest smoothing lengths in model V0256 correspond to 2×10^{-3} pc, while the grid resolution of model P1024 is 4×10^{-2} pc and that of P8192 is 5.3×10^{-3} pc.

The SPH models tend to show a broader post-shock region (greenish colours) than the grid models. The densities for V0256 and P1024 are scaled identically (between $-0.7 < \log n < 3.5$) as well as the temperatures (between $1.0 < \log T < 4.4$). V0256 clearly shows thinner filaments, but at approximately the same density range as model P1024 – a consequence of the density-dependent spatial resolution of SPH.

Fig. 2 shows a zoom sequence of models V0256 (left) and P8192 (right). The spatial extent of each zoom level is indicated in the lower left of the respective panel. The spatial resolution of model P8192 (5.3×10^{-3} pc) is only a factor of 2 away from resolving the Field length (Field 1965) for a realistic value of the heat conductivity (Koyama & Inutsuka 2004). A closer study of the corresponding temperature maps (not shown) indicates that the cooling length, especially between the warm ambient and cold dense gas, is resolved in P8192: the cold dense regions start to show 'haloes' of intermediate-temperature material.

Comparing V0256 and P8192 at the largest scale ($L = 19$ pc), it is already obvious that the SPH model reaches higher densities, at a more filamentary appearance. Conversely, structures in P8192 seem to be more extended and less filamentary. This changes when moving to smaller scales (down to 2 pc). V0256 exhibits mostly coherent filaments at high densities ($n > 10^2$ cm^{-3}), while P8192 shows a whole population of small cloudlets including turbulent wakes. These are conspicuously absent in V0256. Thus, while the density-dependent spatial resolution allows for higher density contrasts and smaller structures in V0256, the constant spatial resolution in P8192 leads to a better tracking of small low-density structures. The differences suggest (compared to the density ranges in Fig. 1) that VINE reaches an effective grid resolution in the dense gas of 1024^2 for (initially) 256^2 particles. The highest zoom also suggests that the density contrasts are more sharply resolved in P8192 than in V0256, leading to smoother gradients in the SPH model.

The highly structured 'slab' of model P8192 and a comparison with P1024 shown in Fig. 1 emphasizes the importance of resolution for the problem of turbulent thermal fragmentation: only at high Reynolds numbers, a turbulent cascade can develop. PROTEUS runs with a specified viscosity, measuring $\nu = 8.9 \times 10^{22}$ cm^2 s^{-1} for our parameters. Using half the period of the geometric perturbation in the collision interface as a typical length-scale, and the inflow velocity as typical flow velocity, results in a formal Reynolds number of $Re \approx 1.6 \times 10^3$ for P1024 and $Re \approx 1.3 \times 10^4$ for P8192. Since the condensation mode of the TI responsible for the fragmentation grows first on the smallest scales (Burkert & Lin 2000), the generation of small-scale structures due to turbulence on which the TI can feed will be crucial for the overall evolution of the system.

3.2 Mass fractions

Fig. 3 shows the mass per length for the cold thermally stable regime ($T < 300$ K), the warm thermally unstable regime ($300 < T < 3000$ K) and the warm thermally stable regime ($3000\,\mathrm{K} < T$), as a function of time. For both codes, the mass of cold gas increases nearly linearly with time once the TI has set in. Thus, despite all its substructure, the interaction zone acts like a one-dimensional slab in terms of mass collection. The slight offset in time between the SPH and grid models is caused by the stronger effect of the artificial (bulk) viscosity in SPH to prevent the penetration of particle layers. The gas thus reaches higher temperatures and requires more time to arrive at densities beneficial for strong cooling (and mass accumulation).

This leads to a constant mass offset of $\approx 70\,\mathrm{M}_\odot\,\mathrm{pc}^{-1}$ in the cold gas between PROTEUS and VINE models, corresponding to $\approx 20\,\mathrm{M}_\odot\,\mathrm{pc}^{-1}$ less intermediate-temperature gas and $\approx 50\,\mathrm{M}_\odot\,\mathrm{pc}^{-1}$ less high-temperature gas in the PROTEUS models. Mass histories of models P4096 and P8192 are indistinguishable.

© 2011 The Authors, MNRAS **415,** 271–278
Monthly Notices of the Royal Astronomical Society © 2011 RAS

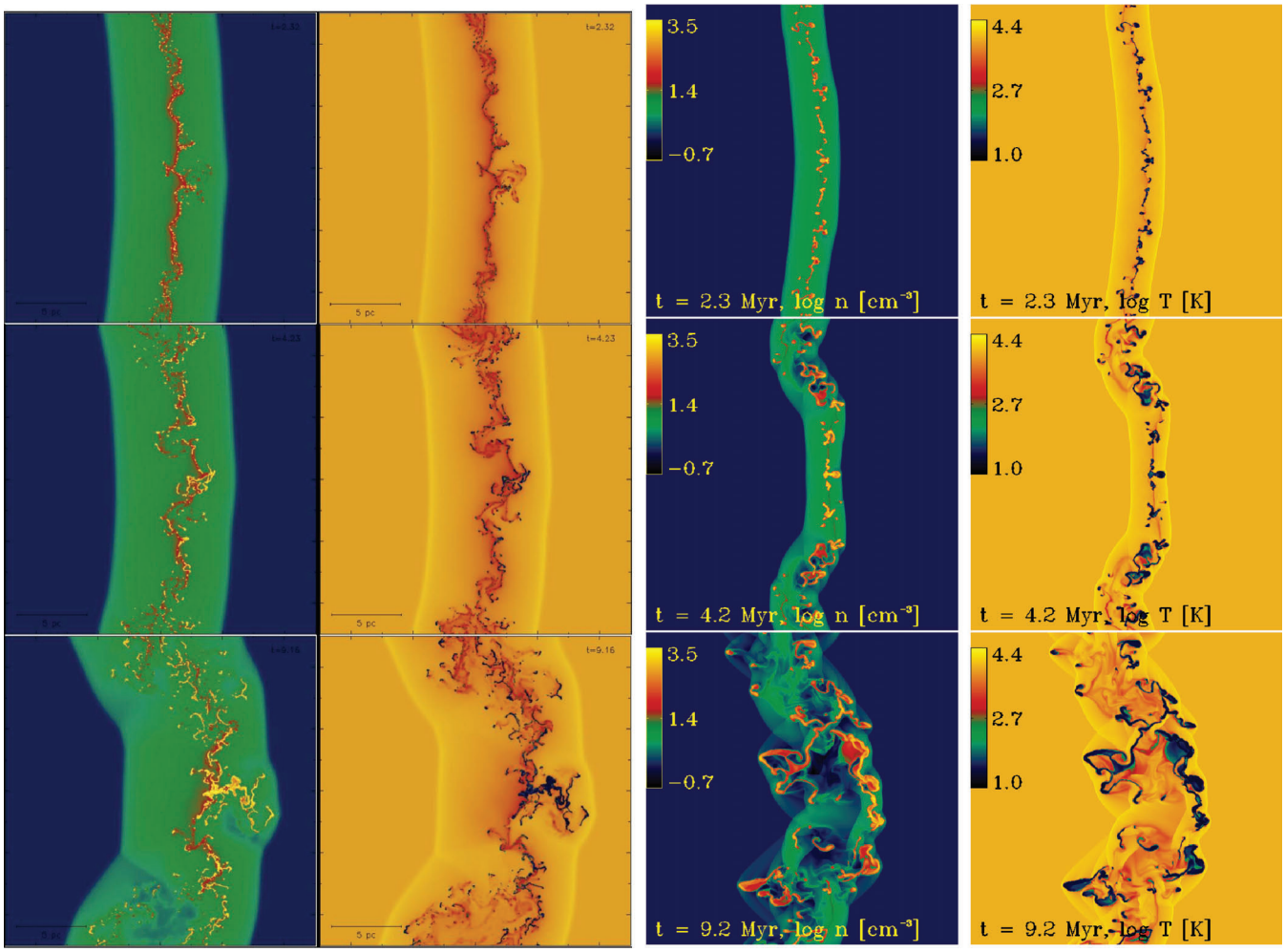

Figure 1. Morphologies of colliding flows. Shown are logarithmic density and temperature maps of the central quarter of the simulation domain, at times $t = 2.3, 4.2$ and 9.2 Myr, for model V0256 (left) and for model P1024 (right). The effective spatial resolution of V0256 leads to more filigree structure than in model P1024, with fixed resolution. Densities are scaled identically between $-0.7 < \log n < 3.5$ for both models and temperatures between $1.0 < \log T < 4.4$. At the stage of proof corrections it was pointed out that the full domain is shown for model P1024.

While the SPH models show less mass in the cold temperature regime, there is more mass in the intermediate and warm regimes. Both codes evolve the warm and intermediate regimes qualitatively similarly: the mass in both regimes stays approximately constant, since they are only transitory stages of the gas on its way to the cold regime.

Considering the widely differing numerical methods, the mass fractions agree surprisingly well. Especially the problem of overcooling in SPH methods (Pearce et al. 1999) does not seem to dominate the mass budget.

3.3 Clump mass function

The strong fragmentation due to the TI begs the question what the resulting clump mass function (ClMF)[1] of the cold clouds will be. While the detailed physical processes linking the ClMF to the core mass function and eventually to the initial mass function are still a matter of debate (e.g. Klessen & Burkert 2000; Williams et al. 2000; Padoan & Nordlund 2002; Ballesteros-Paredes et al. 2006; Elmegreen 2007; Hennebelle & Audit 2007; Dib et al. 2008; Smith, Clark & Bonnell 2009), a model of rapid star formation in colliding flows should explain which physical processes are setting the ClMF during the formation of the MC. The two main fragmentation agents are cooling and self-gravity, the latter of which we have not implemented in the current models. While we envisage self-gravity to be important on global scales (Burkert & Hartmann 2004; Hartmann & Burkert 2007) for finite clouds (i.e. non-periodic boundaries), on local scales, the gas has to cool substantially before the Jeans lengths get small enough for gravity to dominate. Which mechanism then dominates setting the ClMF? Because of the early and strong fragmentation due to thermal (and turbulent) effects, the ClMF might well be determined early on in the cloud evolution [see also Hennebelle et al. (2007) for 2D models and Heitsch et al. (2008a) for 3D models].

The main strength of VINE over PROTEUS is of course the adaptive spatial resolution. To identify clumps of cold gas in model V0256, we have used a friends-of-friends algorithm with a linking length of 0.04 pc, which is about 10 times the minimum kernel softening length at this time and a minimum of 20 particles per clump. In total, we found 418 individual clumps of gas with temperatures

[1] We use the abbreviation ClMF to distinguish between clump and core mass functions, the latter of which is usually abbreviated as CMF in the literature.

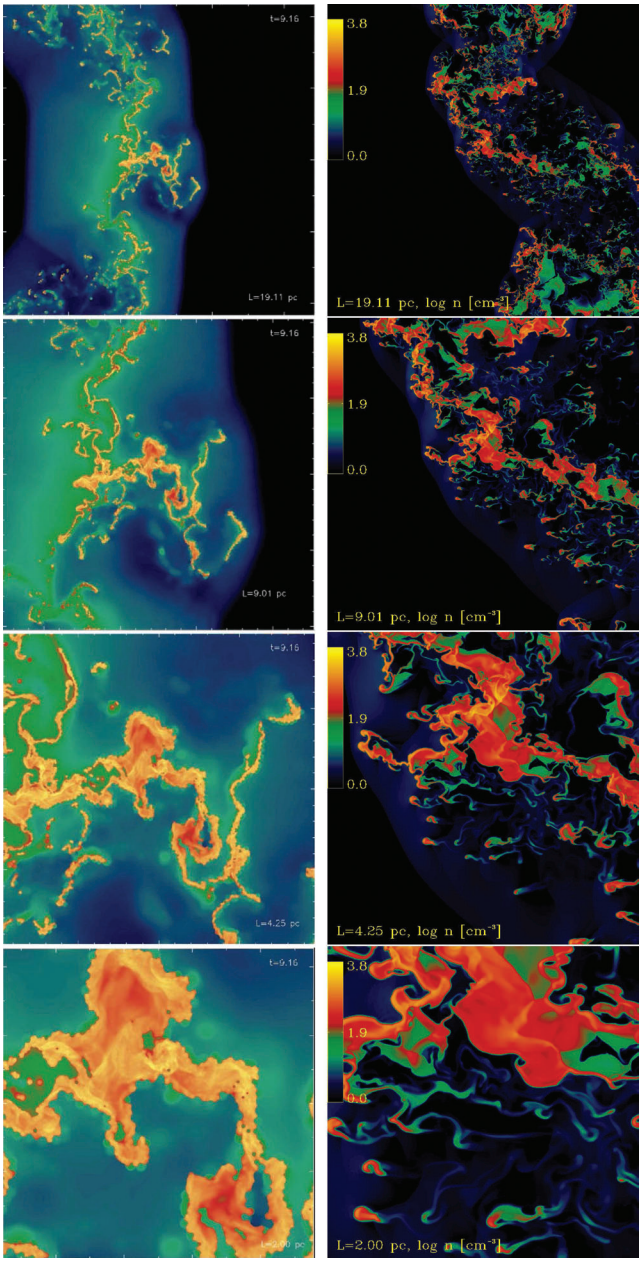

Figure 2. Zoom sequence of V0256 (left) and P8192 (right), logarithm of density, shown at $t = 9.2$ Myr, at (from top to bottom) a scale of 19, 9, 4.25 and 2 pc. Colour scales are identical for both models, highlighting the differences. The full simulation domain would measure 44 pc a side. The smallest dense structures (at a zoom of 2.0 pc) have a size of <0.1 pc. Turbulent wakes are clearly visible in model P8192.

$T < 300$ K. The ClMF is plotted in Fig. 4, at a model time of 9.2 Myr. For comparison, we have computed the ClMFs of models P2048, P4096 and P8192 using the same method. Instead of particle positions, we used the cell positions of the cold gas as input for the friends-of-friends algorithm, again with a linking length of 0.04 pc. For the PROTEUS models, the linking length is a factor of 2–8 larger than the (linear) cell size. As expected, the number of identified clumps increases for the grid simulation with resolution (153 clumps for P2048, 495 for P4096 and 860 for P8192). At high masses, P8192 and V0256 agree, whereas there is a clear deficit in clumps at lower masses for the grid models, with a factor of 3 difference between V0256 and P8192 at $M \approx 1\,\mathrm{M}_\odot\,\mathrm{pc}^{-1}$.

A direct comparison of our ClMF to observations is problematic, for two reasons. First, the restriction to two dimensions will emphasize compression (cooling) over shear flows and vorticity (turbulence) since the gas flows are more compressible than in three dimensions (see fig. 13 of Heitsch et al. 2006). Secondly – as the referee pointed out – we chose to calculate ClMFs at a time (9.2 Myr) at which a sufficient amount of gas will have accumulated for self-gravity to affect the evolution of the cloud. This can be seen comparing models Hf1 and Gf1 of Heitsch & Hartmann (2008, see their fig. 2) at (their) 9.9 Myr. We chose this rather late time for our two-dimensional models, since the suppression of the third dimension leads to rather coherent sheet filaments still imprinted by the initial conditions at earlier times.

Keeping the above caveats in mind, the SPH slope is consistent with the clump mass slopes found by Li et al. (2007) (see also fig. 23 of Ragan, Bergin & Gutermuth 2009) for Orion and with earlier measurements by Heithausen et al. (1998) or Schneider et al. (2002). Overall, the slopes of both methods are shallower than those observed for low-mass star-forming regions such as Perseus (Curtis & Richer 2010). Yet these authors point out that such differences might well be caused by the way in which clumps are defined, since different clump-finding algorithms can result in very different slopes. In any case, for the reasons given above, our argument here focuses more on the comparison between the numerical methods (for which we use the identical clump-finding mechanism) rather than on a detailed comparison with observations.

3.4 Line-of-sight velocity distributions

In Fig. 5, we show the mass-weighted line-of-sight velocity distribution of the cold gas ($T < 300$ K) taken along the inflow direction. The velocity dispersion is $\approx$6.8 km s^{-1} for VINE and $\approx$8.5 km s^{-1} for PROTEUS. The sound speed of the cold gas is $c_\mathrm{s} \approx 0.75$ km s^{-1} at $T = 40$ K, i.e. the cold gas motions are nominally supersonic.

While the overall agreement of the distributions is reassuring, the differences are caused by resolution effects. At higher resolution, smaller scales start to thermally fragment first (e.g. Burkert & Lin 2000), suppressing the growth of the dynamical instabilities (e.g. Vietri, Ferrara & Miniati 1997; Hueckstaedt 2003). Since the SPH models have higher spatial resolution in their evolved state, we expect them to be more dominated by thermal effects rather than by the dynamical instabilities, thus leading to a (slightly) smaller velocity dispersion (see also Heitsch et al. 2005). Also, we expect the generally higher dissipative nature of SPH compared to grid methods (e.g. Kitsionas et al. 2009) to contribute.

With the sound speed in the cold gas $c_\mathrm{s} \approx 0.75$ km s^{-1}, the internal velocity dispersion of the cold clumps turns out to be mostly subsonic (Fig. 6). This confirms earlier findings from numerical simulations (Koyama & Inutsuka 2002; Audit & Hennebelle 2005; Heitsch et al. 2006) and should not come as a surprise in view of the formation mechanism of the cold dense clumps. The PROTEUS models have a broader distribution of internal velocity dispersions than the VINE models, and the peaks shift to smaller velocities with increasing resolution, indicating that the thermal length-scales are not completely resolved at the lowest resolutions (see also Hennebelle & Audit 2007). The distribution for the V0256 clumps is much narrower and peaks around 0.25 km s^{-1}. For comparison, we show the distribution of the internal sound speeds of the individual clumps in Fig. 7. Both distributions peak around 0.45–0.50 km s^{-1}. However, the clumps in the SPH simulations tend to cluster

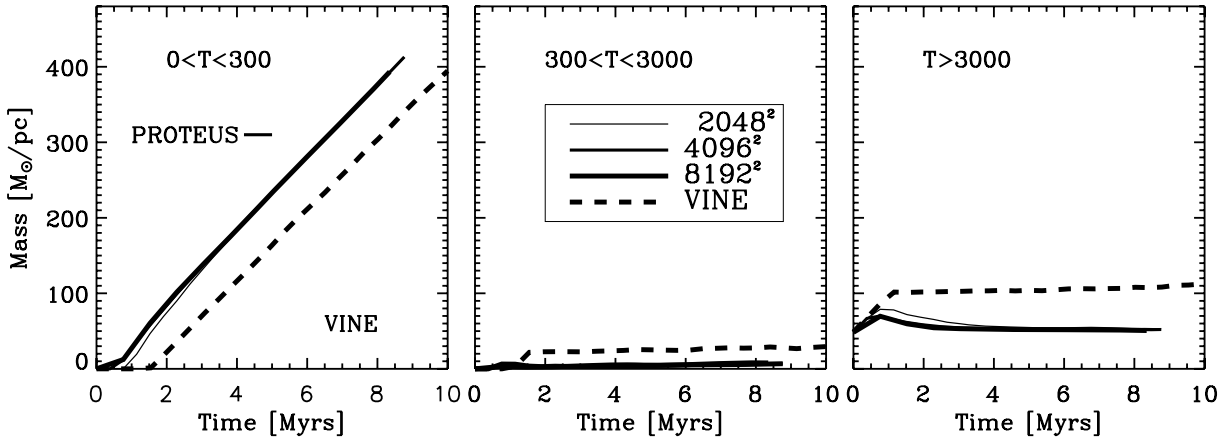

Figure 3. Total mass per length in the three temperature regimes $T < 300$ K, $300 < T < 3000$ K and $3000\ \mathrm{K} < T$ as a function of time. Solid thick lines denote the grid models P2048, P4096 and P8192, while the dashed line shows model V0256. Mass histories for models P4096 and P8192 are indistinguishable. The constant mass offset between VINE and PROTEUS models is due to the higher artificial viscosity in VINE.

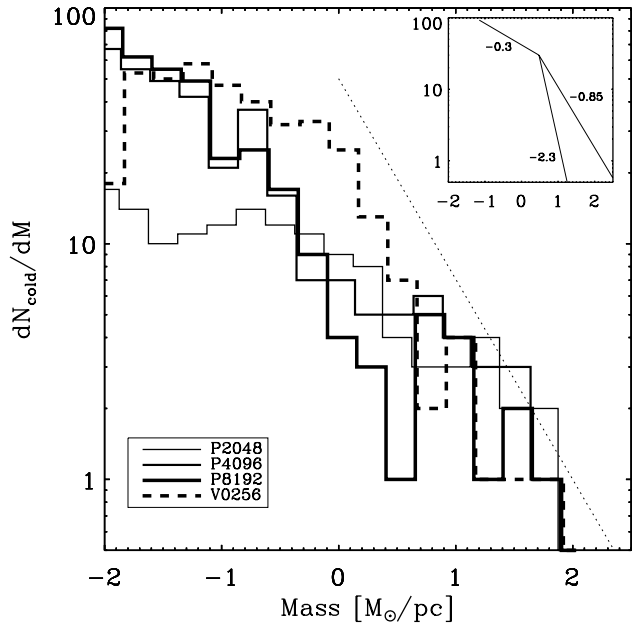

Figure 4. Histogram of clump masses (ClMF) for VINE (V0256, dashed line) and PROTEUS (P2048, P4096, P8192, solid lines), at $t = 9.2$ Myr. The dotted line shows a slope of -0.85 as determined for massive clumps in the Orion MC (Li et al. 2007).

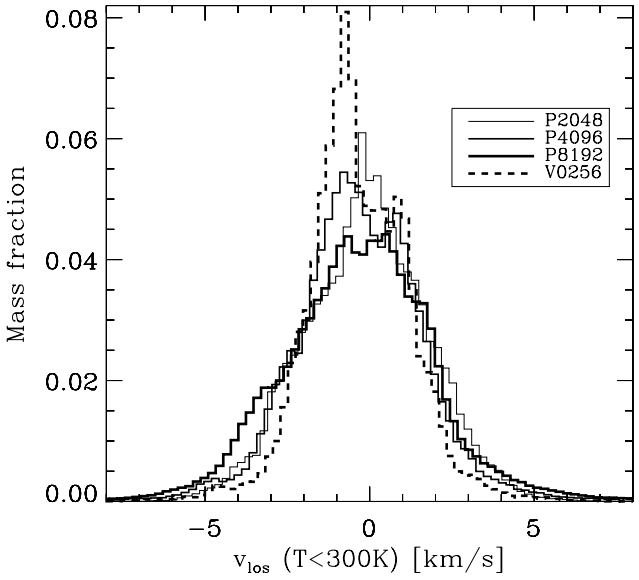

Figure 5. Line-of-sight velocity distribution of the cold gas ($T < 300$ K) along the inflow direction. Dashed line: VINE, solid line: PROTEUS.

at lower temperature ($T < 100$ K) and there is less gas at higher temperatures than in the grid simulations (Fig. 8). This is probably a result of SPH intrinsic overcooling.

4 SUMMARY AND CONCLUSIONS

Lagrangian hydrodynamical methods such as SPH are an attractive tool to simulate astrophysical problems with a wide range of spatial scales, such as self-gravitating objects or thermally unstable flows. However, due to the numerical implementations, the reliability of SPH for such applications has been questioned. We compare an SPH implementation (VINE; Nelson et al. 2009; Wetzstein et al. 2009) and a grid-based method (PROTEUS; Prendergast & Xu 1993; Slyz & Prendergast 1999; Xu 2001; Heitsch et al. 2004) in an application to flow-driven MC formation. This is a challenging astrophysical problem for any numerical method, because of the turbulence, the high-density and -temperature contrasts, and the rapidly shrinking scales of the cold clouds.

The morphologies between particle- and grid-based methods agree well globally, yet the cold gas structures are more fragmented in the SPH models (Fig. 1). Temperature and density gradients in SPH tend to be 'rounder' than in the grid method as a consequence of deriving physical quantities by averaging over a set of nearest neighbours. However, this drawback is countered by the higher spatial resolution, yielding more filigree structure in the SPH models.

The mass fractions of gas in different temperature regimes differ slightly (Fig. 3). SPH models start collecting mass in the cold stable regime later than the grid models, leading to a constant offset in the mass with time. This is a consequence of the strong overheating in the initial flow collision due to SPH's artificial viscosity. The slopes of the ClMFs (Fig. 4) are consistent with results from earlier numerical models (Hennebelle et al. 2007) with similar physics. They are also consistent with observational results (Schneider et al. 2002; Li et al. 2007; Ragan et al. 2009), yet such a comparison should not

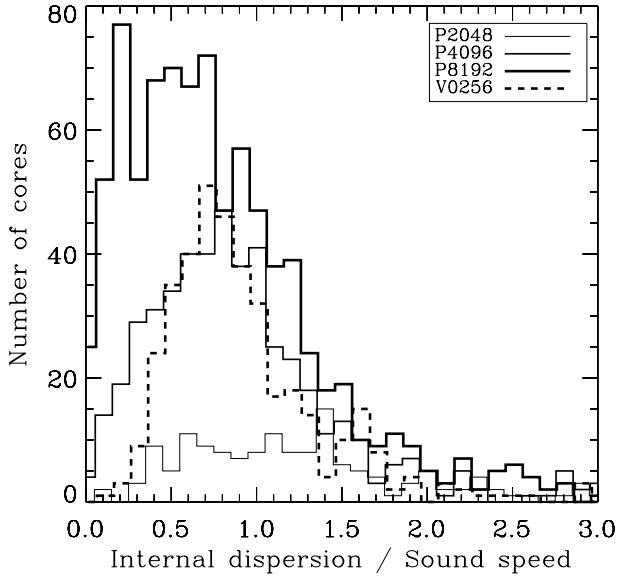

Figure 6. Ratio of internal velocity dispersion to internal sound speed (i.e. the internal Mach number) for all cold clumps. For all models, most of the clumps have subsonic internal motions.

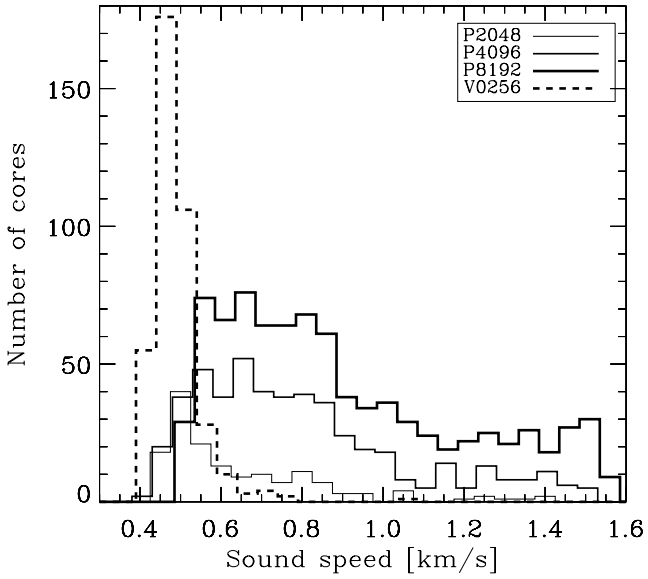

Figure 7. Internal sound speed of the cold clumps ($T < 300$ K). The clumps found in model V0256 have systematically lower internal dispersions with a smaller spread.

be overinterpreted because of the restricted dimensionality of our models as well as the fact that self-gravity will have affected the evolution of the cloud at the time we chose to analyse the models (Heitsch & Hartmann 2008).

The line-of-sight velocity distributions have similar widths (Fig. 5), namely $\approx$6.8 km s^{-1} for VINE and $\approx$8.5 km s^{-1} for PROTEUS, rendering the gas nominally supersonic, while both methods find that the internal velocity dispersion of the cold clumps is subsonic (see also Koyama & Inutsuka 2002; Audit & Hennebelle 2005; Heitsch et al. 2006). The slightly narrower distribution for SPH is a consequence of the higher resolution, emphasizing the thermal instabilities over the dynamical ones.

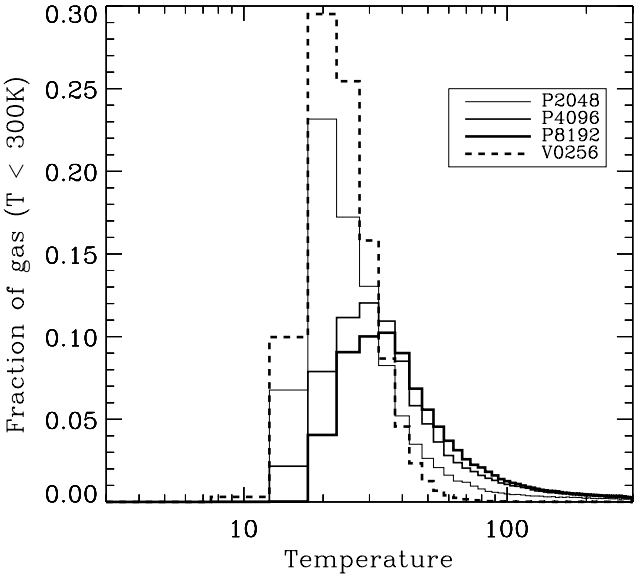

Figure 8. Fractional mass as a function of temperature in the cold phase (not limited to clumps). There is relatively more low-temperature ($T <$ 40 K) gas in model V0256 than in the PROTEUS models.

The effects of overcooling (Pearce et al. 1999) do not seem to affect the overall mass budget (Fig. 3) within the cold stable regime, but they do manifest themselves in the low-temperature tail of that phase (Figs 7 and 8). This suggests that the TI controlling the transition from the warm stable to the cold stable regime is not strongly affected.

Our results suggest that the SPH implementation in VINE is suitable to model thermally bistable, dynamical environments such as occurring in the flow-driven formation of MCs. Yet, quantitative predictions will slightly differ between particle and grid methods, with a bias of the VINE results to lower temperatures and smaller fragments in the cold gas, but a lower total mass in the cold, thermally stable regime compared to PROTEUS. In terms of mass spectra, an initial particle resolution of 256^2 is (at later stages) equivalent to or better than a fixed grid of 4096^2 cells, with promising consequences for the determination of e.g. ClMFs.

ACKNOWLEDGMENTS

We thank the anonymous referee for a very helpful report that led to a clearer focus of the paper. We thank G. Novak for pointing out a mistake in Fig. 1. Simulations were run on the SGI-Altix at the University Observatory Munich, partly funded by the DFG cluster of excellence 'Origin and Structure of the Universe', and on the local PC cluster Star of the Department of Astronomy at the University of Michigan, maintained by J. Hallum. FH acknowledges support of the University of Michigan, of the NASA grant NNG06GJ32G and of the NSF grant AST 0807305. SW acknowledges the support of the Marie Curie RTN CONSTELLATION (MRTN-CT-2006-035890).

REFERENCES

Abel T., 2010, (arXiv:1003.0937)
Agertz O. et al., 2007, MNRAS, 380, 963
André P., Belloche A., Motte F., Peretto N., 2007, A&A, 472, 519
Audit E., Hennebelle P., 2005, A&A, 433, 1
Ballesteros-Paredes J., 2006, MNRAS, 372, 443

Ballesteros-Paredes J., Hartmann L., Vázquez-Semadeni E., 1999, ApJ, 527, 285
Ballesteros-Paredes J., Gazol A., Kim J., Klessen R. S., Jappsen A.-K., Tejero E., 2006, ApJ, 637, 384
Banerjee R., Vázquez-Semadeni E., Hennebelle P., Klessen R. S., 2009, MNRAS, 398, 1082
Bate M. R., Bonnell I. A., Bromm V., 2003, MNRAS, 339, 577
Bisbas T. G., Wünsch R., Whitworth A. P., Hubber D. A., 2009, A&A, 497, 649
Burkert A., Hartmann L., 2004, ApJ, 616, 288
Burkert A., Lin D. N. C., 2000, ApJ, 537, 270
Combes F., Gerin M., 1985, A&A, 150, 327
Curtis E. I., Richer J. S., 2010, MNRAS, 402, 603
Dib S., Brandenburg A., Kim J., Gopinathan M., André P., 2008, ApJ, 678, L105
Dobbs C. L., Bonnell I. A., 2007, MNRAS, 376, 1747
Dobbs C. L., Bonnell I. A., Pringle J. E., 2006, MNRAS, 371, 1663
Dobbs C. L., Glover S. C. O., Clark P. C., Klessen R. S., 2008, MNRAS, 389, 1097
Elmegreen B. G., 1993, ApJ, 419, L29
Elmegreen B. G., 2000, ApJ, 530, 277
Elmegreen B. G., 2007, in Kang Y. W., Lee H.-W., Leung K.-C., Cheng K.-S., eds, ASP Conf. Ser. Vol. 362, The Seventh Pacific Rim Conference on Stellar Astrophysics, The Initial Mass Function of Stars. Astron. Soc. Pac., San Francisco, p. 269
Elmegreen B. G., Lada C. J., 1977, ApJ, 214, 725
Falgarone E., Phillips T. G., 1990, ApJ, 359, 344
Field G. B., 1965, ApJ, 142, 531
Gritschneder M., Naab T., Burkert A., Walch S., Heitsch F., Wetzstein M., 2009, MNRAS, 393, 21
Gritschneder M., Burkert A., Naab T., Walch S., 2010, ApJ, 723, 971
Hartmann L., 2003, ApJ, 585, 398
Hartmann L., Burkert A., 2007, ApJ, 654, 988
Hartmann L., Ballesteros-Paredes J., Bergin E. A., 2001, ApJ, 562, 852
Heithausen A., Bensch F., Stutzki J., Falgarone E., Panis J. F., 1998, A&A, 331, L65
Heitsch F., Burkert A., Hartmann L. W., Slyz A. D., Devriendt J. E. G., 2005, ApJ, 633, L113
Heitsch F., Hartmann L., 2008, ApJ, 689, 290
Heitsch F., Zweibel E. G., Slyz A. D., Devriendt J. E. G., 2004, ApJ, 603, 165
Heitsch F., Slyz A. D., Devriendt J. E. G., Hartmann L. W., Burkert A., 2006, ApJ, 648, 1052
Heitsch F., Hartmann L. W., Slyz A. D., Devriendt J. E. G., Burkert A., 2008a, ApJ, 674, 316
Heitsch F., Hartmann L. W., Burkert A., 2008b, ApJ, 683, 786
Hennebelle P., Audit E., 2007, A&A, 465, 431
Hennebelle P., Audit E., Miville-Deschênes M.-A., 2007, A&A, 465, 445
Hennebelle P., Banerjee R., Vázquez-Semadeni E., Klessen R. S., Audit E., 2008, A&A, 486, L43
Hernquist L., Katz N., 1989, ApJS, 70, 419
Hueckstaedt R. M., 2003, New Astron., 8, 295
Junk V., Walch S., Heitsch F., Burkert A., Wetzstein M., Schartmann M., Price D., 2010, MNRAS, 407, 1933
Karl S. J., Naab T., Johansson P. H., Kotarba H., Boily C. M., Renaud F., Theis C., 2010, ApJ, 715, L88
Kitsionas S. et al., 2009, A&A, 508, 541
Klessen R., 1997, MNRAS, 292, 11
Klessen R. S., Burkert A., 2000, ApJS, 128, 287
Klessen R. S., Heitsch F., Mac Low M.-M., 2000, ApJ, 535, 887
Koyama H., Inutsuka S.-I., 2002, ApJ, 564, L97
Koyama H., Inutsuka S.-I., 2004, ApJ, 602, L25
Lacey C. G., Fall S. M., 1985, ApJ, 290, 154
Larson R. B., 1981, MNRAS, 194, 809
Li D., Velusamy T., Goldsmith P. F., Langer W. D., 2007, ApJ, 655, 351
McCray R., Kafatos M., 1987, ApJ, 317, 190
Mac Low M.-M., Klessen R. S., 2004, Rev. Modern Phys., 76, 125
Mayer L., Quinn T., Wadsley J., Stadel J., 2002, Sci, 298, 1756
Mihos J. C., Hernquist L., 1996, ApJ, 464, 641
Mirabel I. F., 1982, ApJ, 256, 112
Monaghan J. J., 1989, J. Comput. Phys., 82, 1
Monaghan J. J., 1992, ARA&A, 30, 543
Naab T., Jesseit R., Burkert A., 2006, MNRAS, 372, 839
Naab T., Johansson P. H., Ostriker J. P., Efstathiou G., 2007, ApJ, 658, 710
Nagamine K., Cen R., Hernquist L., Ostriker J. P., Springel V., 2005, ApJ, 627, 608
Nelson A. F., Wetzstein M., Naab T., 2009, ApJS, 184, 326
Nigra L., Gallagher J. S. III, Smith L. J., Stanimirović S., Nota A., Sabbi E., 2008, PASP, 120, 972
Padoan P., Nordlund Å., 2002, ApJ, 576, 870
Pearce F. R. et al., 1999, ApJ, 521, L99
Prendergast K. H., Xu K., 1993, J. Chemical Phys., 109, 53
Price D. J., 2008, J. Comput. Phys., 227, 10040
Ragan S. E., Bergin E. A., Gutermuth R. A., 2009, ApJ, 698, 324
Rampp M., Mueller E., Ruffert M., 1998, A&A, 332, 969
Read J. I., Hayfield T., Agertz O., 2010, MNRAS, 405, 1513
Roberts W. W. Jr, Huntley J. M., van Albada G. D., 1979, ApJ, 233, 67
Schneider N., Simon R., Kramer C., Stutzki J., Bontemps S., 2002, A&A, 384, 225
Slyz A., Prendergast K. H., 1999, A&AS, 139, 199
Slyz A. D., Devriendt J. E. G., Silk J., Burkert A., 2002, MNRAS, 333, 894
Smith R. J., Clark P. C., Bonnell I. A., 2009, MNRAS, 396, 830
Springel V., 2000, MNRAS, 312, 859
Springel V., Hernquist L., 2003, MNRAS, 339, 289
Steinmetz M., 1996, MNRAS, 278, 1005
Vázquez-Semadeni E., Ryu D., Passot T., González R. F., Gazol A., 2006, ApJ, 643, 245
Vázquez-Semadeni E., Gómez G. C., Jappsen A. K., Ballesteros-Paredes J., González R. F., Klessen R. S., 2007, ApJ, 657, 870
Vietri M., Ferrara A., Miniati F., 1997, ApJ, 483, 262
Walch S., Burkert A., Whitworth A., Naab T., Gritschneder M., 2009, MNRAS, 400, 13
Walch S., Naab T., Whitworth A., Burkert A., Gritschneder M., 2010, MNRAS, 402, 2253
Wetzstein M., Nelson A. F., Naab T., Burkert A., 2009, ApJS, 184, 298
Williams J. P., Blitz L., McKee C. F., 2000, Protostars and Planets IV. Univ. Arizona Press, Tucson, AZ, p. 97
Wolfire M. G., Hollenbach D., McKee C. F., Tielens A. G. G. M., Bakes E. L. O., 1995, ApJ, 443, 152
Wolfire M. G., McKee C. F., Hollenbach D., Tielens A. G. G. M., 2003, ApJ, 587, 278
Xu K., 2001, J. Comput. Phys., 171, 289
Yang C.-C., Gruendl R. A., Chu Y.-H., Mac Low M.-M., Fukui Y., 2007, ApJ, 671, 374

This paper has been typeset from a TEX/LATEX file prepared by the author.